

Experimental determination of the speed of sound in cavitating flows

Hiva Shamsborhan · Olivier Coutier-Delgosha ·
Guy Caignaert · Fadi Abdel Nour

Received: 12 January 2010/Revised: 26 February 2010/Accepted: 6 April 2010/Published online: 28 April 2010
© Springer-Verlag 2010

Abstract This paper presents measurements of the speed of sound in two-phase flows characterized by high void fraction. The main objective of the work is the characterization of wave propagation in cavitating flows. The experimental determination of the speed of sound is derived from measurements performed with three pressure transducers, while the void fraction is obtained from analysis of a signal obtained with an optical probe. Experiments are first conducted in air/water mixtures, for a void fraction varying in the range 0–11%, in order to discuss and validate the methods of measurement and analysis. These results are compared to existing theoretical models, and a nice agreement is obtained. Then, the methods are applied to various cavitating flows. The evolution of the speed of sound according to the void fraction α is determined for α varying in the range 0–55%. In this second configuration, the effect of the Mach number is included in the spectral analysis of the pressure transducers' signals, in order to take into account the possible high flow compressibility. The experimental data are compared to existing theoretical models, and the results are then discussed.

1 Introduction

The speed of sound in cavitating flows varies significantly according to the local void fraction α . Actually, it is close to 1,500 m/s in pure water, 400 m/s in the vapor, and it may decrease drastically in the liquid/vapor mixture, according to the theoretical model proposed by Jakobsen (1964). This implies that cavitating flows are nearly incompressible in areas of pure liquid, and highly compressible in two-phase flow regions. In configurations of high-speed flows occurring, for example, in pumps or injectors, the Mach number in the liquid/vapor mixture is expected to increase up to 10, whereas it is close to zero outside the mixture. Transition between these two behaviors may be abrupt, because of high local density gradients.

This large amplitude of compressibility variations in cavitating flows is of paramount importance for the understanding of their unsteady behavior, since it may be involved in the mechanism of periodical vapor shedding associated with cloud cavitation. Actually, it has been suggested by several authors that pressure waves resulting from cloud collapse downstream from a pump blade or a hydrofoil may have some influence on the unsteady behavior of the sheet cavities, which is observed in such situations (Arndt et al. 2000; Leroux et al. 2005). It has been shown, for example, by Leroux et al. (2005) in a configuration of cloud cavitation on a 2D foil section that different types of periodical cavitation cycles are obtained according to the intensity of the pressure wave emitted during the implosion of the cloud of vapor.

Therefore, taking into account the compressibility of the flow in numerical simulations is necessary to reproduce some complex mechanisms associated with cavitation instabilities. However, this requires a correct estimation of the local speed of sound in the cavitating medium. For

Electronic supplementary material The online version of this article (doi:10.1007/s00348-010-0880-6) contains supplementary material, which is available to authorized users.

H. Shamsborhan (✉) · O. Coutier-Delgosha · G. Caignaert ·
F. Abdel Nour
Arts et Metiers ParisTech/Laboratoire de Mécanique de Lille
(UMR 8107), 8 boulevard Louis XIV, 59046 Lille Cedex, France
e-mail: hiva_sh@yahoo.com

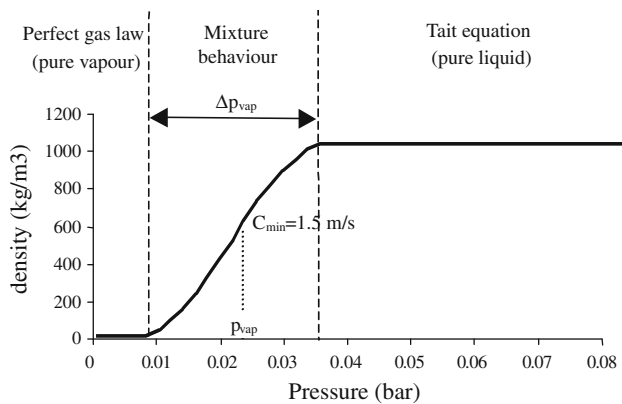


Fig. 1 Barotropic state law used for numerical simulation in water by Coutier-Delgosha et al. (2003)

example, some cavitation models are based on a barotropic state law that controls the density variations of the mixture according to the local pressure evolution (see for example Delannoy and Kueny 1990; Merkle et al. 1998; Coutier-Delgosha et al. 2003). In such models (Fig. 1), the local slope S of the state law is directly linked to the local speed of sound by Eq. (1).

$$c^2 = \frac{\partial P}{\partial \rho} = \frac{1}{S} \quad (1)$$

The speed of sound c in Eq. (1) is either the isentropic or the isothermal one. Indeed, Gouse and Brown (1964) have shown that for any liquid/gas two-phase flow, both speeds are nearly identical if m_g is negligible in comparison with m_l , where m_g and m_l are the gas and liquid mass, respectively, in the measurement volume V .

In the numerical simulations based on such barotropic state law, the maximal slope S_{\max} is a crucial parameter, as it controls the thickness and the internal structure of the sheet cavity. Therefore, it should be consistent with the physics. At the present time, its value has been usually obtained from the theoretical model proposed by Jakobsen (1964), which gives a minimal speed of sound c_{\min} close to 3.3 m/s for cold water (20°C). The final value used in the numerical simulations by Coutier-Delgosha et al. (2003) is $c_{\min} = 1.5$ m/s, in order to obtain sheet cavity shapes similar to the ones observed in the experiments.

However, no consensus currently exists concerning the c_{\min} value and more generally regarding the evolution of c according to the volume fraction of the vapor phase β . The initial model proposed by Jakobsen (1964) and revisited by Wallis (1969) is based on the respective compressibility of the vapor and the liquid: if a volume V containing a mass m of liquid and vapor is submitted to a pressure variation ΔP , then the respective volume variations of vapor and liquid can be calculated, and the resulting volume variation can be obtained, which results in the following formula:

$$\frac{1}{c^2} = \frac{1}{c_v^2} \left[\beta^2 + \beta(1-\beta) \frac{\rho_l}{\rho_v} \right] + \frac{1}{c_l^2} \left[(1-\beta)^2 + \beta(1-\beta) \frac{\rho_v}{\rho_l} \right] \quad (2)$$

where c_v , c_l , and c are the speeds of sound in the pure vapor, in the pure liquid, and in the liquid/vapor mixture, respectively, ρ_v and ρ_l denote the densities in pure vapor and pure liquid, and β is the volume fraction of the vapor phase.

In expression (2), mass and heat transfers are neglected, so it can be applied to any gas/liquid mixture, in so far as no major effect due to vaporization or condensation must be taken into account. This may not be the case for cavitating flows; therefore, Eq. (2) may not be valid for such complex mixtures that never reach equilibrium.

Another model has been proposed by Nguyen et al. (1981) for configurations of diluted gaseous phase in the liquid. These authors obtain a slightly different expression of the speed of sound in the medium, as can be observed in Fig. 2 in the case of a water/air mixture at temperature 20°C and atmospheric pressure. Note that for both models, the speed of sound in the mixture depends implicitly on the local pressure through the variations of the gas density ρ_g and the speed of sound in the gaseous phase c_g according to the pressure.

More recently, Brennen (2005) has proposed more complete expressions of the speed of sound in two-phase mixtures: mass and heat exchanges are taken into account. However, calibration of the mass and heat exchanges requires some further experimental investigations. Concerning the heat transfer in single-component two-phase mixtures, two extreme solutions are considered: “homogeneous equilibrium model”, i.e. instantaneous thermal equilibrium between the two phases, and “homogeneous frozen model”, which assumes zero transfer between them.

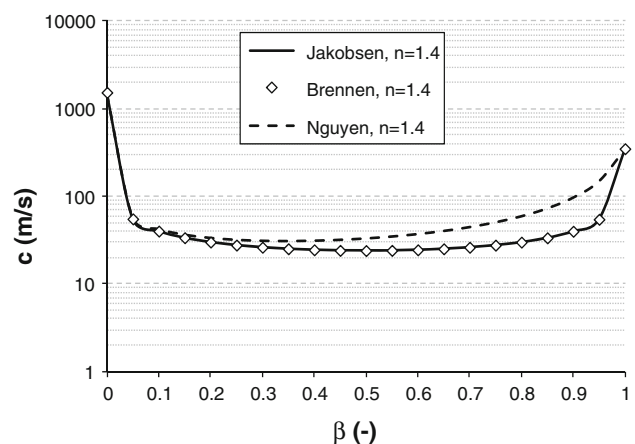


Fig. 2 Comparison of theoretical models for the speed of sound in air/water mixture according to volume fraction of the air. (Logarithmic scale, atmospheric pressure at 20°C, adiabatic process)

It is shown by Brennen (2005) that experimental results usually lay between these two solutions. If mass transfers are neglected, the following relation is obtained by Brennen:

$$\frac{1}{c^2} = (\beta\rho_g + (1 - \beta)\rho_l) \cdot \left(\frac{\beta}{n \cdot P} + \frac{1 - \beta}{\rho_l \cdot c_l^2} \right) \quad (3)$$

where n is the polytropic index and P is the pressure in both phases if surface tension is neglected. It can be checked that expressions (2) and (3) are equivalent.

Some experiments devoted to the measurement of the wave propagation speed in two-phase flows are also reported in the literature. Testud et al. (2007) have investigated cavitation downstream from a diaphragm, and they have measured the speed of sound with a method based on three pressure transducers. A minimal speed of 13 m/s has been found by these authors, but the associated void fraction was not measured. Experiments in stratified air/water flows are also reported by Henry et al. (1971): propagation time of a pressure wave between two cross-section is measured with two piezo-electric transducers. Measurements in air/water mixtures were also performed by Costigan and Whalley (1997), using a single pressure transducer that detects the propagation of a pressure wave generated by the closure of inlet air and water valves. Time propagation of the wave enables to derive its speed in the liquid/gas medium. Results have been obtained for a void fraction varying between 0 and 50%, and a good agreement with the model proposed by Brennen was shown.

The present study consists of experiments whose basic aim is to measure the evolution of the speed of sound c according to the void fraction α in a cavitating flow. The speed of sound is defined by Eq. (1), while the void fraction α is obtained in any point according to expression 4:

$$\alpha(M) = \Delta t_k / \Delta t \quad (4)$$

where Δt_k is the time of presence of phase k at point M during the time Δt .

However, the technique for the determination of the speed of sound is not local, since it is based on the signal analysis of three piezo-electric transducers. Consequently, a volume V of flow characterized by nearly constant physical properties is required in order to perform space-averaged measurements of wave propagation speed. The main challenge of the present work was thus related to the creation of a homogeneous volume V of cavitating flow, i.e. a volume containing a liquid/vapor mixture characterized by a small space variation of the void fraction. Simultaneous measurements of c and $\bar{\alpha}$ were performed, where $\bar{\alpha}$ denotes the mean value of α in the volume V :

$$\bar{\alpha}(V) = \int_V \alpha \cdot dV \quad (5)$$

The value $\bar{\alpha}$ is obtained by space averaging local measurements performed with an optical probe. Not only cavitating flows (single-component two-phase mixture) but also air/water flows (two-component two-phase flows) were investigated in this study, in order to validate the experimental technique.

For the purpose of these experiments, an existing cavitation tunnel of the LML (Laboratoire de Mécanique de Lille, France) has been equipped with a Plexiglas test section in order to visualize cavitation. A grid is located perpendicular to the flow upstream from the test section, in order to obtain cavitation in its wake. For investigation into air/water flows, an air injection device through a circular ring located in the flow upstream from the test section has also been installed. A honeycomb structure is used to obtain the best homogeneity of the two-phase flow in the test section. The experimental test facility and instrumentation are detailed in Sect. 2. The methods used to measure the void fraction and the speed of sound, including their validation in air/water flow configurations, are presented in Sects. 3 and 4, respectively. Section 5 is devoted to the experimental results obtained in cavitating flows and the subsequent analysis and discussion.

2 Experimental setup

An existing cavitation tunnel at the LML laboratory has been modified for the present experiments (Fig. 3). The test facility is mainly composed of an axial pump driven by an electrical motor and two tanks. The nominal volume flow rate and net power of this axial pump are respectively 0.092 m³/s and 5,800 W. Tank 1 (downstream from the pump) is full of water, while tank 2 (upstream from the pump) has a free surface. Pressure in the installation can be decreased from the atmospheric pressure down to

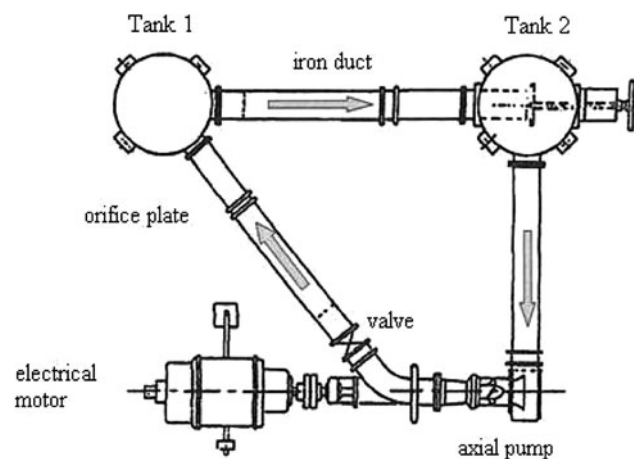


Fig. 3 Scheme of the cavitation tunnel

200 mbar, using a vacuum pump connected to tank 2. The water volume flow rate in the cavitation tunnel can be varied according to the rotation speed of the axial pump (from 950 up to 1,600 rpm) and also by opening more or less a valve located between the pump and tank 1 (Fig. 3). The volume flow rate of water is measured with a Rosemount differential pressure sensor connected to two pressure taps located inside and downstream of the orifice plate indicated in Fig. 3. The measurement uncertainty of this device is estimated to $\pm 6.5\%$.

For the purpose of the present experiments, the initial iron duct between tanks 1 and 2 has been replaced by a cylindrical Plexiglas test section. As detailed hereafter, two successive test sections, of diameter 14 and 5 cm, respectively, have been used.

2.1 Test section 1

The internal diameter of the test section 1 is 14 cm. Air/water mixture can be obtained inside by air injection through a circular ring located inside the upstream convergent (Fig. 4). The compressed air source is the laboratory network. The air volume flow rate, which can be varied by modifying the injection pressure, is measured

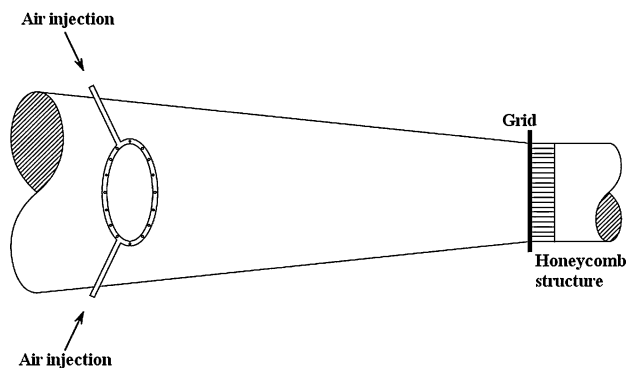


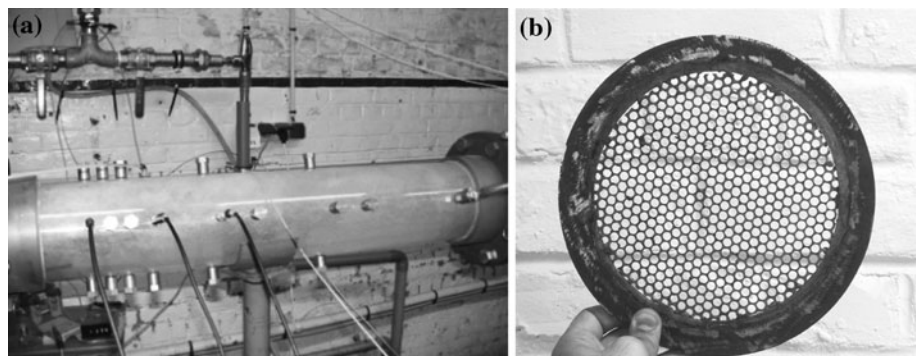
Fig. 4 Scheme of the air injection method for air/water (test section 1)

with a flowmeter. This one is calibrated for air at atmospheric pressure, so appropriate corrections are applied to take into account the effect of the injection pressure. For experiments in cavitating flows, wake cavitation is created behind a grid installed perpendicular to the flow upstream from the test section (Fig. 5). The grid is 3 mm thick, and it is composed of 500 holes whose average diameter is 5.7 mm. To obtain cavitation, the pressure is decreased in the tunnel down to 200 mbar.

In this configuration, the maximum available volume flow rate Q_1 is 60 l/s, which corresponds to a mean velocity in the Plexiglas tube close to 3.9 m/s. The maximum volume flow rate of air Q_a is limited by the injection device. So, to reach high void fractions in air/water flow configurations, the water volume flow rate is reduced down to 26 l/s by decreasing the rotation speed of the circulation pump down to 1,000 rpm. The resulting mean velocity of water is close to 1.7 m/s. In such situation, the Reynolds number based on the tube diameter is $Re = 2.4 \times 10^5$, so the flow is fully turbulent. If Q_1 was still reduced, a stratified two-phase flow would be obtained in the test section, which would modify the speed of sound: indeed, Nguyen et al. (1981) have shown the difference of pressure wave propagation between a stratified two-phase flow and a homogeneous one.

Taps for pressure sensors and the optical probe are manufactured in several cross-sections (see Fig. 6), in order to enable various measurement stations within the two-phase mixture. Three cross-sections located, respectively, 18, 28, and 38 cm downstream from the grid are investigated in the present study. They will be denoted hereafter stations 1, 2, and 3, respectively. Each one is equipped with four taps: (1) one is connected to a Rosemount pressure sensor that gives the time-averaged local pressure with relative uncertainty 0.5%, (2) one is used for the optical probe, whose tip can be moved from $r = 0$ (center of the test section) to $r = 6.5$ cm (close to the wall), (3) the two last taps are used for hydrophones or piezo-electric pressure transducers, for the measurement of the speed of sound (see Sect. 3).

Fig. 5 a Test section 1, b grid that generates cavitation



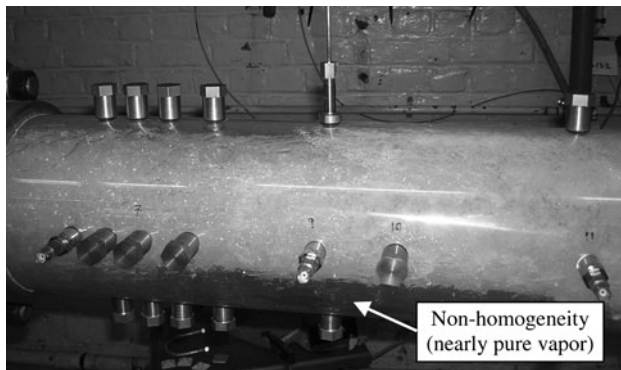


Fig. 6 Cavitating flow (test section 1)

Test section 1 has been used in the first part of the study for the calibration of the void fraction measurements with the optical probe, in situations of air/water two-phase flows (Sect. 3). Then, it has been found not appropriate to measurements in cavitating flows, since the two-phase structure downstream from the grid is not homogeneous, as can be observed in Fig. 6. Consequently, a 10-cm-long honeycomb structure was added at the inlet of the test section, but only minor improvement was obtained, as will be shown in Sect. 4. Thus, a second test section of smaller diameter was manufactured.

2.2 Test section 2

The internal diameter of the second test section is 5 cm. It will be demonstrated in Sect. 3 that the two-phase flow obtained after this modification is characterized by a fair homogeneity. The test section is also manufactured in Plexiglas, it is 78 cm long, and it is equipped with the same taps as test section 1. In order to integrate this test section in the cavitation tunnel, new convergent and divergent pieces are mounted upstream and downstream as shown in Fig. 7.

Two grids of thickness 2 mm have been used to create cavitation in test section 2 (Fig. 8). Grid 1 is composed of 69 holes whose diameter is 5 mm. It results in cavitating flows characterized by high void fractions but low mean velocity of water, because of the supplementary head losses generated by the grid obstruction. To obtain flows with higher velocity, grid 2 was used: it is composed of 19 holes whose diameter is 10 mm. The measurements are performed in various cross-sections located between 20 and 60 cm downstream from the grid.

All results presented in Sects. 4 and 5 of the present paper were obtained in flow configurations generated in test section 2.

3 Measurement of the void fraction

The optical probe technique and signal post-processing applied for the determination of the space-averaged void

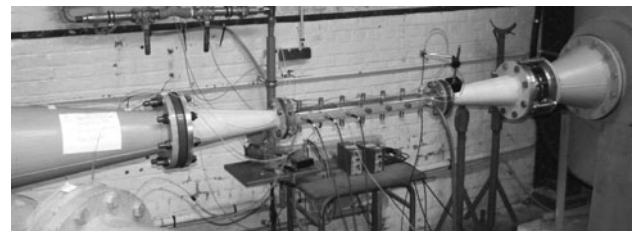


Fig. 7 Test section 2

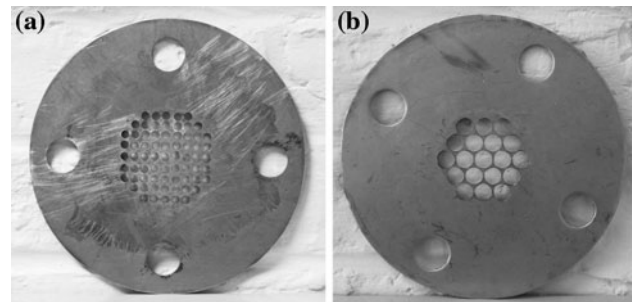


Fig. 8 a Grid 1, b grid 2 (test section 2)

fraction $\bar{\alpha}$ in the volume V where the speed of sound is measured are presented in this section. The validation of this process is also included.

3.1 Signal acquisition

The determination of the local void fraction α is based on optical probe measurements. This technique has been already used in many situations of two-phase flows, and it was applied previously to air/water and cavitating flows by Gabillet et al. (2002) and Stutz and Reboud (1997), respectively. It is based on the Snell Descartes law. Infrared light is emitted inside the optical probe, and then a part of this light is reflected back from the tip of the probe and measured. The intensity of the refracted light depends on the index of refraction of the medium surrounding the probe. The refractive indices of liquid and gas are different, which enables the phase detection on the probe signal. The optical signal is converted to an electronic one through the optoelectronic module, and then it is recorded on a computer with LABVIEW.

According to previous definition (4), the void fraction $\alpha(M)$ at point M is the ratio of the gas-phase residence time to the experiment duration time T_{exp} . Given T_{gi} the residence time of the i th gas structure crossing M :

$$\alpha(M) = \lim_{T_{\text{exp}} \rightarrow \infty} \frac{\sum T_{gi}}{T_{\text{exp}}} \quad (6)$$

The residence time of the gas bubbles is obtained with a single threshold technique, as proposed by Stutz and Reboud (1997): when a gas bubble passes on the probe tip,

detection of both interfaces is based on a single signal level, which is a percentage of the signal amplitude (Fig. 9). In the present study, the optical probe is equipped with a sapphire tip of diameter 80 μm . The signal of the probe was recorded during a time $T = 15$ s at frequency 100 kHz, which results in 1.5 millions of points per acquisition. These data were post-processed with Matlab.

3.2 Calibration for air/water two-phase flows

In the present work, the optimal threshold was determined in a configuration of air/water two-phase flow. The calibration process is based on the comparison between the space-averaged void fraction $\bar{\alpha}$ derived from optical probe measurements in a cross-section and the volume fraction of the gaseous phase β calculated from the measured air and water volume flow rates. This comparison requires the two following assumptions: (1) the flow is axisymmetric, so the void fraction is investigated along one radius of the cross-section only, (2) the flow is globally steady, i.e. no large-scale fluctuations affect the two-phase area, which has been checked by visual observation. The measurements with the optical probe are performed in the cross-section located at station 2 of test section 1. Values of the void fraction are obtained at points located on a radius, for r varying between zero and 6.5 cm by steps of 0.5 cm. Then, the mean void fraction in the cross-section is calculated by space averaging the local values, according to Eq. (7):

$$\bar{\alpha} = \frac{\sum_i \alpha_i \cdot \pi \cdot ((r_i + \delta r)^2 - (r_i - \delta r)^2)}{\pi \cdot R^2} \quad (7)$$

where R is the test section radius, r_i is a radius where the measurement is performed, and δr equals 0.25 cm, excepted at the axis tube and close to the wall.

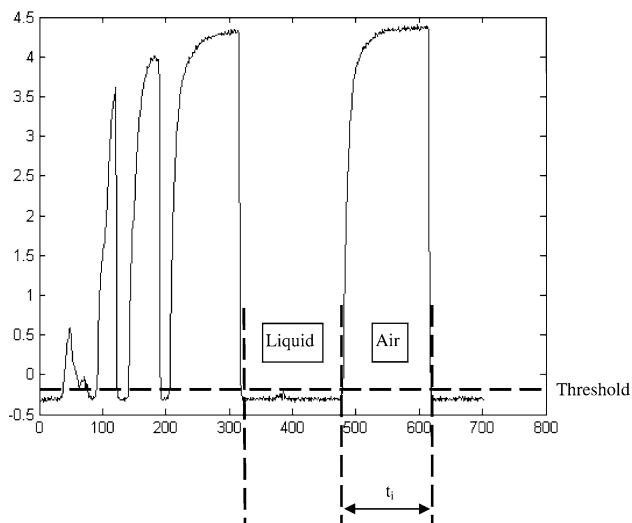


Fig. 9 Example of signal from the optical probe

The measured air volume flow rate is corrected according to the local pressure in the cross-section and the perfect gas law (Eq. 8), and the volume fraction of the gaseous phase is calculated according to Eq. (9).

$$\frac{Q_{\text{air}}^{\text{test section}}}{Q_{\text{air}}^{\text{flowmeter}}} = \frac{P_{\text{injection}}}{P_{\text{bubbles}}} \quad (8)$$

$$\beta = \frac{Q_{\text{air}}^{\text{cross section}}}{Q_{\text{water}} + Q_{\text{air}}^{\text{cross section}}} \quad (9)$$

where $P_{\text{injection}}$ and P_{bubbles} refer to the pressure in the air flowmeter and inside the air bubbles at station 2 of the test section, respectively, while $Q_{\text{air}}^{\text{flowmeter}}$ and $Q_{\text{air}}^{\text{cross section}}$ are the air volume flow rates at the same locations. Note that P_{bubbles} used in Eq. (8) is slightly different from the pressure P_{wall} measured at the wall at station 2, because of the surface tension:

$$P_{\text{bubbles}} = P_{\text{wall}} + \frac{\sigma}{r_a} \quad (10)$$

where $\sigma = 73 \times 10^{-3} \text{ N m}^{-1}$ is the surface tension and r_a is the average radius of the bubbles during the experiment. It is derived from the signal of the optical probe: each bubble diameter d_i is obtained from the passage time t_i of the bubble on the probe (see Fig. 9), according to Eq. (11):

$$d_i = t_i \times V_{\text{moy}} \quad (11)$$

where V_{moy} is the mean flow velocity in the test section.

Values of $\bar{\alpha}$ and β are compared for various volume flow rates of injected air (Fig. 10). For β , a 10% relative uncertainty (reported on the graph) is calculated from the precision of the air flowmeter and Rosemount sensor that are used for the measurements of the flow rates. A precision of 15% was estimated previously regarding the measurements of the void fraction with the optical probe (Stutz and Reboud 1997). Several values of the threshold S are investigated, from 1.2 up to 10% of the signal amplitude. Although in the previous studies, $S = 10\%$ has been

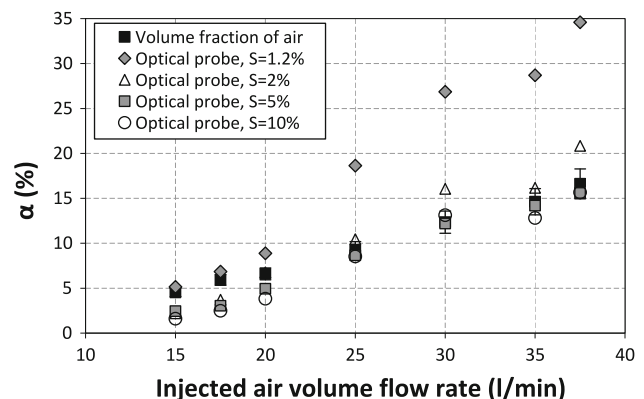


Fig. 10 Calibration of the void fraction measurement. (Test section 1, station 2, air/water two-phase flow)

usually found to be appropriate (Stutz and Reboud 1997), the best agreement is obtained presently in the range 2–5%, as can be seen in Fig. 10. The RMS value related to $\bar{\alpha} - \beta$ is minimized for $S = 5\%$, so this value is applied hereafter for all experiments in air/water flows.

The resulting evolutions of $\bar{\alpha}$ and β according to the injected air flow rate Q_a , at stations 1, 2, and 3, are drawn in Fig. 11. The uncertainties mentioned previously are reported on the charts. As can be seen in Fig. 11, a good general agreement is obtained, which confirms the validity of the calibration. However, it can be noticed that $\bar{\alpha}$ is usually smaller than β for small values of injection rates, especially at stations 2 and 3. For high injection rates, such difference is not observed. This discrepancy may be related to a significant underestimation of the gas volume with the optical probe, because of the small size of bubbles: as a matter of fact, the optical probe is not able to detect the air bubbles with diameters smaller than the thickness of the probe tip ($80\ \mu\text{m}$). Moreover, it is mentioned by Stutz and Reboud (2000) that the probe tip does not even penetrate correctly some bubbles of larger size.

An estimation of the average size of the bubbles according to the radius is given in Fig. 12, at stations 1, 2, and 3, for a low air flow rate $Q_a = 20\ \text{l/min}$. It can be observed that the size of the bubbles close to the center of the test section is similar to the diameter of the probe tip, which suggests that a significant amount of very small bubbles may be contained in water in such configuration. For higher values of air flow rate, the order of magnitude of the mean size of the detected bubbles increases, so it is expected that the amount of very small bubbles is smaller.

It is also observed at station 1 that the discrepancy between both measurements increases drastically when Q_a is higher than 30 l/min. This may be due to spurious cavitation: indeed, the pressure in the cavitation tunnel is decreased down to 200 mbar for the air/water investigations, to obtain larger void fractions. Even if the flow velocity is small, cavitation in the grid wake may be induced by high rate of included air.

4 Measurement of the speed of sound

4.1 Measurement technique

Several methods can be used in order to get experimentally the speed of sound in the liquid/gas medium. One-first category of techniques is based on the use of two transducers: one sound or ultrasound emitter and one receiver, with a measurement of the time delay between them. Such technique enables a quite local measurement, since only the flow between the emitter and the receiver is concerned. It is used, for example, in ultrasonic flowmeters, generally with a periodical excitation of the emitter. However, issues

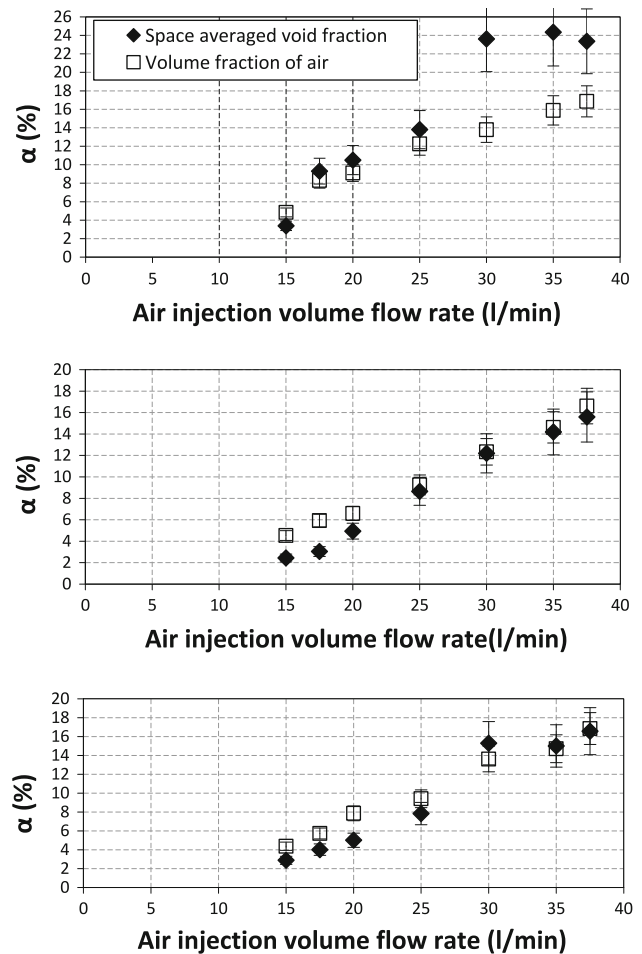


Fig. 11 Comparison between the space-averaged void fraction and the volume fraction of air. Test section 1, stations 1–3 (top to bottom), air/water two-phase flow

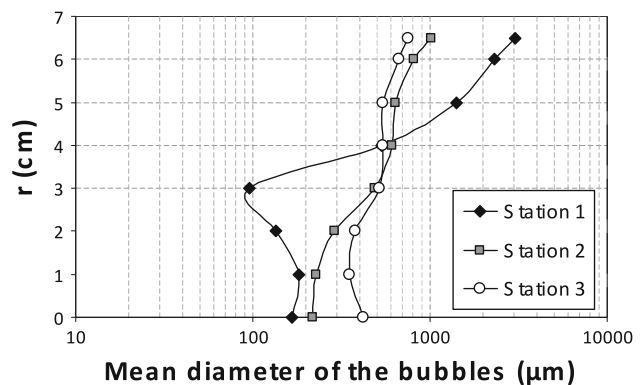


Fig. 12 Estimation of the mean bubble diameter at stations 1, 2, 3 for $Q_a = 20\ \text{l/min}$ (test section 1)

related to this method come from the large variations of the speed of sound which are expected for gas/liquid mixtures with variables void fractions. Measurements are also perturbed by multiple reflections of the incident wave, due to the walls of the tests sections. This is why another method

is used in the present study: three pressure transducers were mounted flush on the Plexiglas test section, at equal distance from each other in the flow direction (Fig. 13). This method was developed by Margolis and Brown (1976) and enables to derive the mass flow rate and the speed of sound from the spectral analysis of the signals given by the three pressure transducers. That technique is rather well known and has been applied successfully, for a long time, to liquid or gas flows in pipes (see for example, Bolpaire 2000). It can be used without external excitation of the flow, as the existing hydro-acoustics sources in systems, due to pumps, valves and other singularities, are sufficient. The effect of the deformability of the pipe wall on the celerity of the waves has usually to be taken into account. The main assumptions related to this method are the following:

- One-dimensional wave propagation in ducts of constant cross-section: it means that the wavelengths of waves propagating in the duct have to be larger than the diameter of the pipe. Consequently, the method applies well in the low-frequency domain.
- The deformability of the pipe wall must be taken into account, assuming that the cross-section remains circular during deformations. The wave celerity c in the infinity must be derived from the apparent wave propagation speed c_0 measured in the pipe, according to the Allievi formula (Wylie and Streeter 1978) given in Eq. (12).

$$c = c_0 \cdot \sqrt{1 + \frac{D}{e \cdot E \cdot \chi} \cdot C_1} \quad (12)$$

where D , e , E , and χ are the pipe diameter, the wall thickness, the Young's modulus of pipe material, and the coefficient of compressibility of the fluid, respectively. Non-dimensional coefficient C_1 is related to the pipe mechanical boundary condition according to its

installation and Poisson ratio of its material. In this work, for both Plexiglas test sections $C_1 = 0.856$.

- Viscous effects are assumed to be negligible.
- The mean flow velocity in the duct is assumed to be much lower than the celerity of the waves (no compressibility effect is taken into account).

With such hypotheses, from the mass and momentum conservation equations for a fluid, the following equation can be obtained in the case of small fluctuations:

$$\tilde{P}(x, t) = C_1 e^{j(\omega t + kx)} + C_2 e^{j(\omega t - kx)} \quad (13)$$

where $\tilde{P}(x, t)$ is the pressure fluctuation at position x , $k = \omega/c_0$ is the wave number, c_0 is the wave celerity in the pipe, and C_1 , C_2 are two coefficients.

This relation can be expressed also in the frequency domain:

$$P(x, f) = C_1(f) e^{jkx} + C_2(f) e^{-jkx} \quad (14)$$

By applying $x = -L, 0, +L$ in Eq. (14) for the three pressure transducers and then combining the three relations, the transfer function H can be written as:

$$H = \frac{1}{2} \frac{P(-L, f) + P(L, f)}{P(0, f)} \quad (15)$$

The real part of H should be periodical and the imaginary part should be zero.

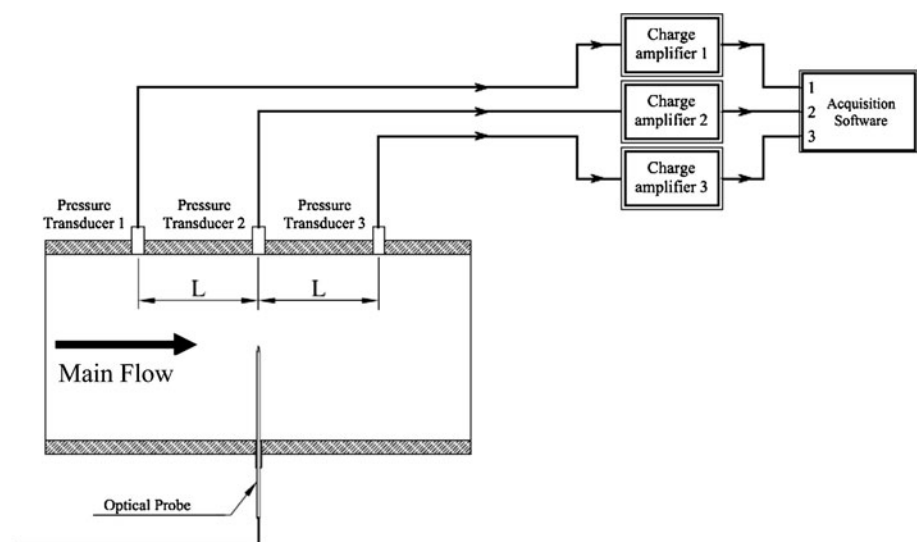
$$Re[H] = \cos\left(\frac{\omega L}{c_0}\right) \quad (16)$$

Thus, the speed of sound can be deduced from the first frequency f_0 for which the real part becomes zero:

$$c_0 = 4f_0 L \quad (17)$$

The speed of sound obtained from Eq. (17) is the propagation speed of plane waves in a pipe, not in the

Fig. 13 Location of the pressure transducers for measurement of the speed of sound



infinity. The wave celerity in the infinity c is obtained from Eq. (12), combined with Eq. (18) which is the definition of c :

$$c = \frac{1}{\sqrt{\rho \cdot \chi}} \quad (18)$$

where $\rho = \beta\rho_g + (1 - \beta)\rho_l$ is the density of the liquid/gas mixture, and ρ_g , ρ_l are the gas and liquid densities, respectively. Note that β is obtained with the optical probe, as detailed in the previous section.

4.2 Signal acquisition

Three Kistler 701A piezo-electric pressure transducers were used for signal acquisition. Their precision is estimated to 1%. To apply the method detailed in the previous section to the calculation of the speed of sound, a cutoff frequency above which the waves do not propagate anymore in the form of plane waves has to be taken into account (Abom and Boden 1988). For test section 1, this frequency is close to 2,100 Hz, so the investigated range of frequency is 0–2,048 Hz. Each recorded signal is the average of 100 acquisitions and is sampled in 4,096 spectral lines according to Shannon sampling requirements. For test section 2, the cutoff frequency is about 10,000 Hz, so the investigated range of frequency is 0–10,240 Hz and the sampling frequency is 20,480 Hz.

In previous applications of this method (Bolpaire 2000), a coherence function was used to eliminate the measurements whose coherence is lower than 0.8. However, in the present experiments, significant vibrations of the test section were observed during the measurements. Indeed, in order to facilitate the installation of the Plexiglas tubes, a dilatation facility is used downstream from the test section. The drawback is a significant increase of the vibrations due to the flow and the vacuum pump, which may perturb the measurements. Bolpaire (2000) pointed out this reason to explain the decrease of the coherence function for some of his results, in a similar configuration of measurement. This is the reason why no condition related to the coherence function is applied in the present study, neither for air/water experiments nor for cavitating ones. This enables to obtain enough points to plot the transfer function (H) and to obtain clearly the value of frequency f_0 .

The records of the signals and the calculation of the transfer and coherence functions are performed with the signal-processing software LMS.

4.3 Validation of the method in water/air configuration

Before performing the experiments in a cavitating flow, the speed of sound is measured in air/water mixtures with various mean void fractions. Air is injected upstream from

the test section (see Sect. 2) and a bubbly flow is obtained. With test section 1, it is observed that the bubbly flow becomes more and more inhomogeneous when the air volume flow rate is increased, in spite of the use of a honeycomb structure between air injection and the Plexiglas tube. Such inhomogeneous flow can be clearly observed for Q_a higher than 20 l/min, as can be seen in Fig. 14, which presents two visualizations of the two-phase flow, for $Q_a = 15$ l/min and $Q_a = 30$ l/min, respectively. Situation obtained in Fig. 14b looks similar to the slug flow regime detailed by several authors such as Brennen (2005). As the transducers are parietal measurement devices, this flow configuration is not appropriate for measurements of the speed of sound.

This issue is confirmed by Fig. 15: quantitative evolutions of the void fraction with the radius of the test section are drawn for the same air injection rates. Radius $r = 0$ is the center of the Plexiglas tube, while radius $r = 7$ cm is the inner wall of the pipe. Results are given at stations 1, 2, and 3. The maximum void fraction in each cross-section is indicated on the charts. It can be observed for $Q_a = 30$ l/min that the void fraction increases drastically at the tip of

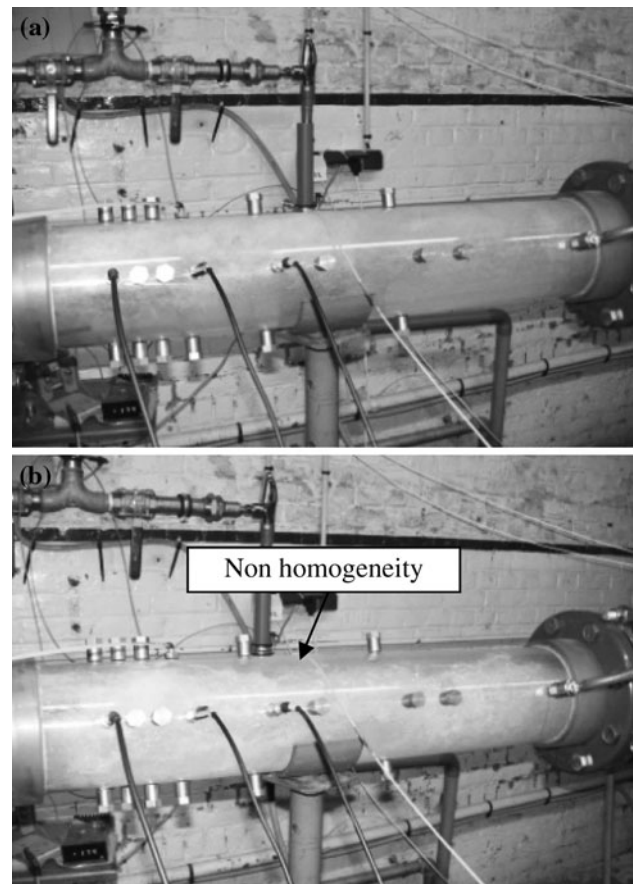


Fig. 14 Air/water flow structure for **a** $Q_a = 15$ l/min, **b** $Q_a = 30$ l/min

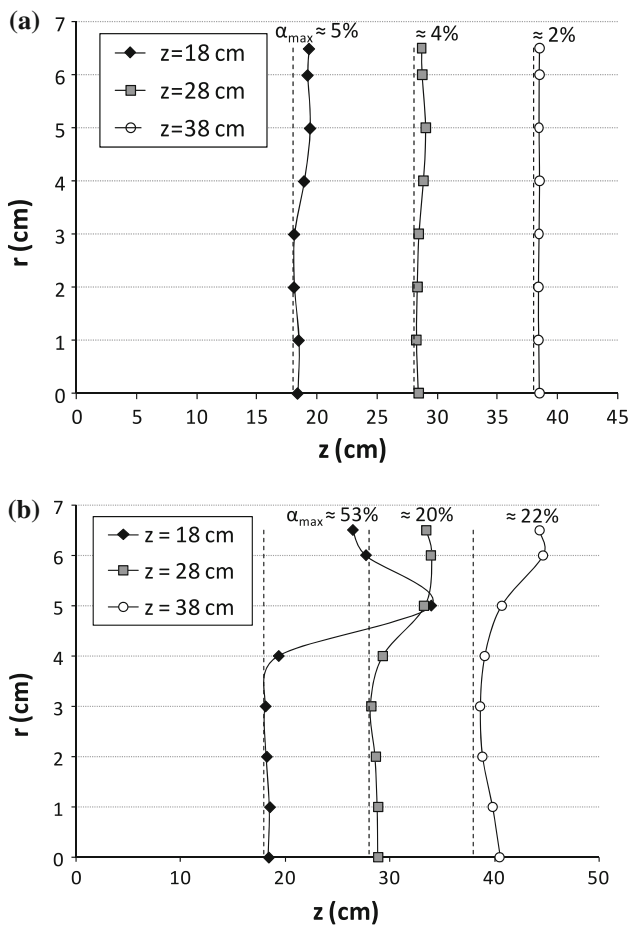


Fig. 15 Distribution of α with radius at stations 1, 2, and 3, with air injection rates **a** 15 l/min, **b** 30 l/min

the test section, for $4\text{ cm} < r < 6\text{ cm}$. This result can be associated with the non-homogeneity observed in Fig. 14b.

Therefore, test section 2 is used for all measurements presented hereafter. The mean void fraction in each cross-section is calculated according to Eq. (7) with measurements of α from $r = 0\text{ cm}$ to $r = 2.25\text{ cm}$ with steps of 3 mm. Charts drawn in Fig. 16 indicate the distribution of void fraction according to the radius for different air flow rates, in a cross-section located 50 cm downstream from the inlet of the test section. It can be observed the homogeneity is much better than previously: the modifications of the void fraction between $r = 0$ and $r = 2.25\text{ cm}$ do not exceed 50%, even for high injection rates, while it was varying between 1% and more than 50% with test section 1. So, it was considered that the two-phase flow homogeneity in this configuration enables to perform measurements of the speed of sound and mean void fraction according to the methods presented previously.

Results are presented in Fig. 17 in logarithmic scale and compared with the theoretical models proposed by Jakobsen (1964) and Nguyen et al. (1981). The models were

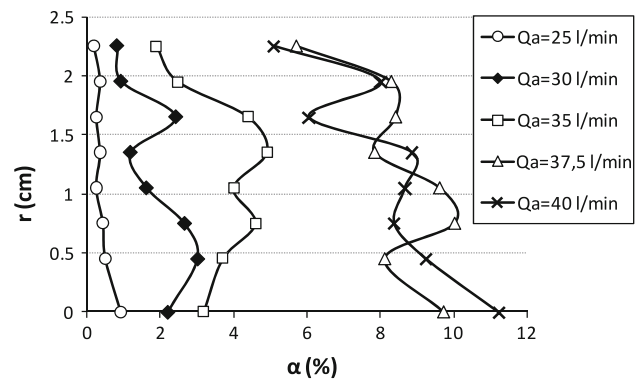


Fig. 16 Distribution of α according to r for different values of Q_a ($z = 50\text{ cm}$, test section 2)

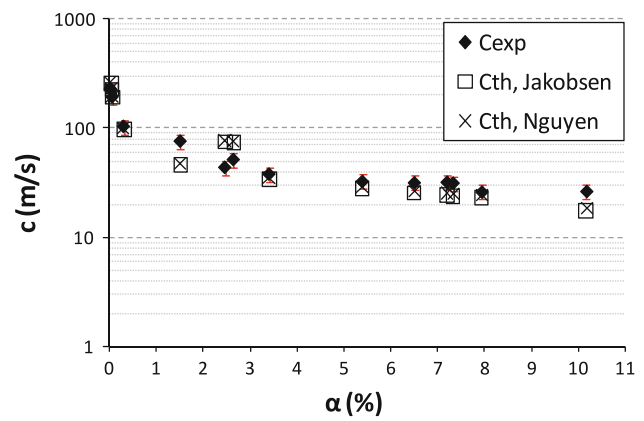


Fig. 17 Speed of sound according to $\bar{\alpha}$. (Air/water mixture, test section 2)

applied with values $c_1 = 1,500\text{ m/s}$ and $\rho_1 = 1,000\text{ kg/m}^3$ for the liquid phase, while the air density ρ_a is calculated by Eq. (19) according to static pressure and $T = 293^\circ\text{K}$. The static pressure is measured for each experiment in the cross-section where the optical probe is located in front and middle of transducers (see Fig. 13).

$$\rho_a = \frac{P}{R \cdot T} \tag{19}$$

with $R = 287\text{ J/kg/K}$.

The speed of sound for air is obtained from Eq. (20):

$$c_a = \sqrt{n \cdot R \cdot T} \tag{20}$$

where $n = 1.4$ is the polytropic index of perfect gas in the case of an adiabatic process. It has been shown by Gouse and Brown (1964) that for an air/water mixture characterized by $\rho_l \gg \rho_a$, the adiabatic speed of sound is less than 3% higher than the isothermal one. So, in the present case, both speeds can be considered as nearly identical.

The maximum void fraction obtained in these experiments is about 10%, which is sufficient to check the nice agreement between the two models and the present

measurements. A 15% mean uncertainty on the celerity values is estimated from the discrepancies between the experimental and theoretical results, as indicated on the experimental chart in Fig. 17. It can be noticed that the minimal speed of sound obtained in the experiments is close to 20 m/s. Since the mean flow velocity is about 2 m/s in this case, the mean Mach number increases up to 0.1, so the hypothesis of incompressible flow used in the method based on the three pressure transducers remains valid in this configuration.

These results confirm that the experimental method developed here for the investigation into the speed of sound enables to perform valid measurements, in spite of the issue reported in the previous section regarding the decrease of the coherence function due to the vibrations of the test section.

5 Results

5.1 Theoretical aspects

In all theoretical models reported in the introduction (Jakobsen 1964; Wallis 1969; Nguyen et al. 1981; Brennen 2005), the speed of sound decreases drastically in the two-phase mixture, compared with each phase separately. This is due to two main reasons:

1. In any liquid/gas mixture, the compressibility is much higher than the one of each component considered separately. This can be understood by considering the effects of applying a pressure variation ΔP to a volume V that contains either pure liquid, pure gas, or a mixture of gas and liquid. The compressibility of the pure liquid volume can be expressed as:

$$\chi_l = \frac{\Delta\rho_l}{\Delta P} = \frac{1}{\Delta P} \left(\frac{m_l}{V'} - \frac{m_l}{V} \right) = \frac{m_l}{\Delta P} \cdot \frac{V'_1 - V}{V \cdot V'_1} \tag{21}$$

where $\Delta\rho_l$ is the density variation due to the pressure variation, V'_1 is the liquid volume after the pressure variation, and m_l is the mass of liquid inside the initial volume V .

For the volume of pure gas, the compressibility has a similar expression:

$$\chi_g = \frac{\Delta\rho_g}{\Delta P} = \frac{1}{\Delta P} \left(\frac{m_g}{V'} - \frac{m_g}{V} \right) = \frac{m_g}{\Delta P} \cdot \frac{V'_g - V}{V \cdot V'_g} \tag{22}$$

with $\Delta\rho_g$ the gas density variation, V'_g the new gas volume, and m_g the mass of gas inside the initial volume V .

In the mixture, the compressibility is the following:

$$\chi = \frac{\Delta\rho}{\Delta P} = \frac{1}{\Delta P} \left(\frac{m}{V'} - \frac{m}{V} \right) = \frac{m}{\Delta P} \cdot \frac{V' - V}{V \cdot V'} \tag{23}$$

where m denotes the mass of the mixture and V' is the new volume of the mixture.

In this last case, m is close to $m_l/2$ (if the gas mass is neglected), while $V' - V$ can be decomposed into:

$$V' - V = \left(V'_g - V_g \right) + \left(V'_1 - V_1 \right) \tag{24}$$

where V'_g and V'_1 are the new volumes of gas and liquid initially contained in V , respectively.

If we define $\psi = \frac{c_l}{c_g}$ the ratio between the gas and the liquid speeds of sound, then the following relation can be obtained:

$$\frac{1}{\psi^2} = \frac{(\partial\rho/\partial P)_l}{(\partial\rho/\partial P)_g} = \frac{m_l}{m_g} \cdot \frac{\partial(1/V)_l}{\partial(1/V)_g} = \frac{m_l}{m_g} \cdot \frac{V_g^2}{V_1^2} \cdot \frac{\partial V_1}{\partial V_g} \tag{25}$$

If the initial volume fraction of gas before pressure variation is β , then $V_g = \beta \cdot V$ and $V_1 = (1 - \beta)V$.

So, the ratio of the volume variations in liquid and in gas can be written as:

$$\frac{V'_1 - V_1}{V'_g - V_g} = \frac{\partial V_1}{\partial V_g} = \frac{m_g}{m_l} \cdot \left(\frac{1 - \beta}{\beta} \right)^2 \cdot \frac{1}{\psi^2} \tag{26}$$

Equation (26) shows that the volume variation of gas is much higher than the liquid one: if $\beta = 0.5$, the ratio is about 6×10^{-5} . So Eq. (23) can be approximated as:

$$\chi = \frac{m}{\Delta P} \cdot \frac{V' - V}{V \cdot V'} \approx \frac{m_l}{\Delta P} \cdot \frac{V'_g - V_g}{V \cdot V'} \tag{27}$$

Equation 27 shows why compressibility in the mixture is much higher than the one in liquid or in gas, by comparison with the results of Eqs. (21) and (22):

- The mass involved in Eq. (27) is the liquid one, which is much higher than the gas one, so $\chi \gg \chi_g$.
- The volume variation is the gas one, which is much higher than the liquid one, so $\chi \gg \chi_l$.

2. In the special case of two-phase flow with mass exchanges, strong density variations can also arise from slight vaporization or condensation due to ΔP .

5.2 Experimental investigations

Measurements in cavitating conditions were performed with test section 2. To reach high void fractions in the cavitating areas, the water mass flow rate was much increased, compared with the experiments reported in the previous section. Therefore, the rotation speed of the circulation pump was increased from 1,000 up to 1,600 rpm. This leads to a significant intensification of electromagnetic field created by electrical motor of the pump, which results in a strong perturbation of the optoelectronic device that converts the optical signal into an electronic one. Consequently, a supplementary noise in the signal of the optical probe is observed, and a non-zero void fraction is obtained

even in pure liquid flow. To get rid of this effect, the threshold level S is set at a higher position: it is progressively increased until $\alpha = 0$ is obtained in pure water (see Fig. 18). The appropriate value is found to be $S = 15\%$. It is applied for all measurements reported hereafter.

The flow homogeneity has been checked for several flow conditions. Void fraction profiles are similar to the ones obtained previously with air injection: no large variation was detected, which confirmed the nice flow homogeneity observed visually.

The mean velocity in the test section slightly depends on the development of cavitation downstream from the grid, since the head losses in the pipe vary significantly according to this parameter. With grid 1 (see Fig. 8), the mean velocity was obtained in the range 3.7–4.6 m/s. A first set of data obtained for various values of mean void fraction was analyzed, and the values of the Mach number M in each case were derived from the measured speed of sound and flow velocity. It can be observed in Fig. 19 that in most of the case, $M > 0.4$, so the compressibility effects should not be neglected in the method used to obtain the speed of sound from the three pressure transducers.

Without taking into account any effect of compressibility, the matrix T_r of the hydro-acoustics transfer between two cross-sections 1 and 2 can be written as follows:

$$\begin{pmatrix} P \\ \rho \cdot c \cdot v \end{pmatrix}_2 = T_r \cdot \begin{pmatrix} P \\ \rho \cdot c \cdot v \end{pmatrix}_1 \quad (28)$$

with $T_r = \begin{bmatrix} \cos(kL) & -j \times \sin(kL) \\ -j \times \sin(kL) & \cos(kL) \end{bmatrix}$

where P and v denote here the Fourier transforms of the pressure and velocity at a given frequency. Expression (28) results in the Eqs. (15–17) given in Sect. 4. According to Miles (1981), the transfer matrix that includes the compressibility effects can be written as follows:

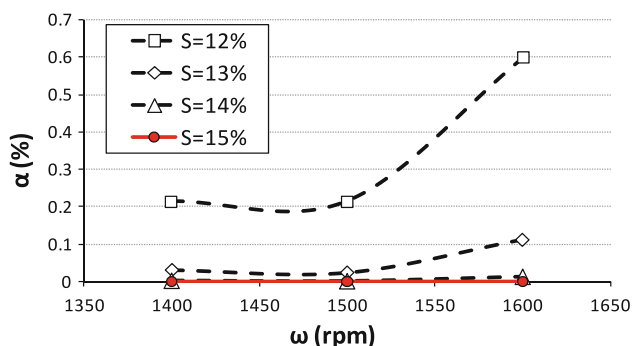


Fig. 18 Measurement of the void fraction with different values of the threshold, for increased rotation speeds of the circulation pump (pure water flow)

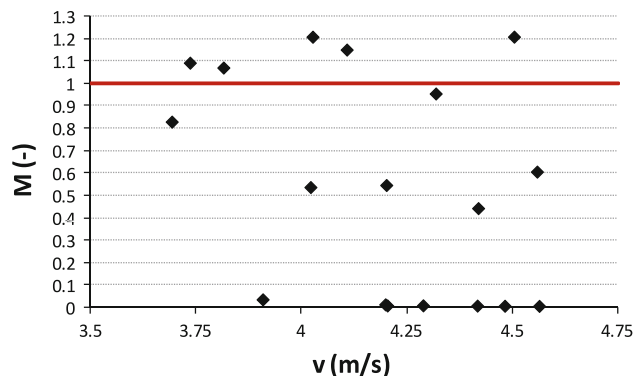


Fig. 19 Mean Mach number according to mean flow velocity. (Cavitating conditions, test section 2, grid 2)

$$T_r = e^{-\xi \cdot M \cdot L} \begin{bmatrix} \cos(\xi L) & -j \times \sin(\xi L) \\ -j \times \sin(\xi L) & \cos(\xi L) \end{bmatrix} \quad (29)$$

where $\xi = k(1 - M^2)$ depends on M and the wave number k . As it can be checked, the transfer matrix defined in Eq. (29) becomes identical to the one defined in Eq. (28) when $M = 0$.

By applying the relation (29) between cross-sections 1 and 2, and between 2 and 3, the following relations are obtained:

$$\begin{pmatrix} P_2 \\ \rho \cdot c \cdot v_2 \end{pmatrix} = \begin{pmatrix} A & -jB \\ -jB & A \end{pmatrix} \begin{pmatrix} P_1 \\ \rho \cdot c \cdot v_1 \end{pmatrix} \quad (30)$$

$$\begin{pmatrix} P_3 \\ \rho \cdot c \cdot v_3 \end{pmatrix} = \begin{pmatrix} A & -jB \\ -jB & A \end{pmatrix} \begin{pmatrix} P_2 \\ \rho \cdot c \cdot v_2 \end{pmatrix} \quad (31)$$

with $A = e^{-\xi \cdot M \cdot L} \cdot \cos(\xi L)$ and $B = e^{-\xi \cdot M \cdot L} \cdot \sin(\xi L)$.

The combination and rearrangement of expressions (30) and (31) lead to the following relation:

$$\frac{P_3}{P_2} + (A^2 + B^2) \frac{P_1}{P_2} - 2A = 0 \quad (32)$$

where $A^2 + B^2 = e^{-2\xi \cdot M \cdot L}$.

By combining the real and imaginary parts of expression (32), Eq. (33) is obtained:

$$F_f - 2A = 0 \quad (33)$$

with $F_f = Re\left(\frac{P_3}{P_2}\right) - \frac{Im\left(\frac{P_3}{P_2}\right)}{Im\left(\frac{P_1}{P_2}\right)} \cdot Re\left(\frac{P_1}{P_2}\right)$.

Equation (33) should be verified for each frequency if included in the spectrum of the experimental measurements, but in practice, the experimental errors systematically lead to non-zero values of $F_f - 2A$. To determine the speed of sound, the following iterative procedure has been applied to the experimental data: (1) a initial value of M is calculated with the incompressible method, (2) the real and imaginary parts of the transfer functions are calculated in the all range of measured frequencies (0–10,240 Hz), using this first value of M , (3) a least square method is used to

find the value of the wave celerity that minimizes the sum, over the frequency range, of $F_f - 2A$. All contributions $F_f - 2A$ that give too high values or the error are suppressed. It has been checked that the removed frequencies include the ones that are higher than the cutoff frequency related to the speed of sound. Indeed, this cutoff frequency decreases drastically in configurations of liquid/vapor mixture. Figure 20 presents a result for a single experimental point: the measured wave celerity is obtained at the minimum of the curve. (4) The calculated speed of sound gives a new Mach number, which is used to calculate a new speed of sound, and the whole process is repeated until the convergence is reached.

A comparison between the results obtained with and without taking into account the compressibility effects is presented in Fig. 21. Speeds of sound are drawn according to the mean void fraction. It can be observed that significant differences are obtained for high values of void fractions, i.e. for values of celerity lower than 4.5. Since the mean flow velocity is close to 4 m/s, it means that compressibility effects should be included in the present analysis when the Mach number becomes higher than 0.9. Consequently, all results presented hereafter take compressibility effects into account for the calculation of c .

The experiments were performed for various values of the pressure in the test section, in order to obtain different extents of the cavitation area and different values of the mean void fraction in each investigated cross-section. Moreover, the device shown in Fig. 13 was successively located in several cross-sections, between 20 and 60 cm downstream from the grid, in order to increase the range of investigated void fractions. The final range is 0–55%.

Speeds of sound measured in cavitating conditions are drawn in Fig. 22, according to the mean void fraction $\bar{\alpha}$. Note that a logarithmic scale is applied in ordinate. The

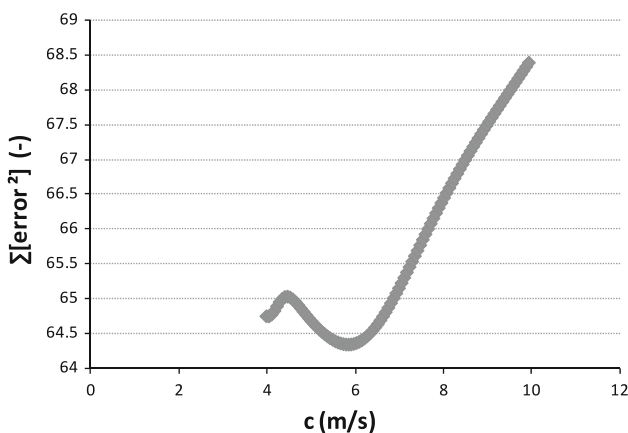


Fig. 20 Determination of the wave celerity. Mean flow velocity 3.7 m/s. Calculation in the incompressible case $c = 4$ m/s. Calculation with compressibility effects $c = 5.8$ m/s

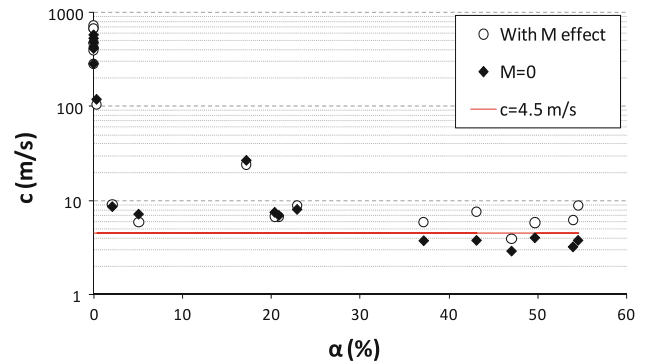


Fig. 21 Comparison of the speeds of sound obtained with/without Mach number effect. (Logarithmic scale in ordinate)

experimental results are compared with the model proposed by Jakobsen (1964) for adiabatic and isothermal processes. The vapor density is derived from Eq. (19) with $R = 462$ J/kg/K for the vapor and $T = 293^\circ\text{K}$. To draw the theoretical values, the mean pressure measured during the experiments in the section where the void fraction is measured (position 2 of the pressure sensors) was used. The polytropic index for vapor equals 1.3 if the process is adiabatic and it equals 1 if it is isothermal. In Fig. 22, the theoretical values for both processes are also indicated with their tendency curves (T.C.). The 15% uncertainty on c calculated previously in air/water configurations is indicated on the experimental chart. However, the uncertainty is expected to increase significantly with cavitating flows: indeed, (1) regarding the determination of the void fraction, the threshold S was increased from 5 up to 15%, to avoid the spurious signal fluctuations induced by the high rotation speed of the circulation pump and the associated vibrations of the test section. (2) The measurement precision of the speed of sound may be also partially deteriorated, because of the vibrations of the Plexiglas tube that reduce the coherence function of the pressure measurements.

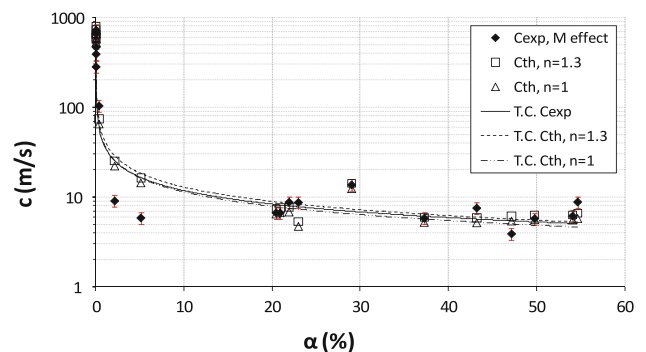


Fig. 22 Speed of sound in cavitating flow according to $\bar{\alpha}$. (Logarithmic scale, grid 1, flow velocity in the range 3.6–4.7 m/s)

It can be observed that the tendency curve derived from the experimental data lies between the tendency curves of the adiabatic and isothermal processes. It shows that the models proposed by Jakobsen (1964) and Brennen (2005) remain valid in the case of cavitating flow, although no mass transfer was considered in these approaches. This result suggests that the density variations associated with the mass transfers may have only a little influence on the compressibility of the liquid/vapor mixture. Conversely, the mechanism detailed in Sect. 5.1 would remain preponderant.

5.3 Effect of the flow velocity

As mentioned before, the cavitating flow obtained in the wake of grid 1, which is characterized by mean velocities close to 4 m/s, does not have a wide range of mean flow velocity. To check the influence of the mean flow velocity on the speed of sound, grid 2 is used instead of grid 1 (see Fig. 8). Holes are bigger, so head losses decrease and the mean flow velocity in the test section can be increased up to 13 m/s. New measurements have been performed with velocity comprised between 7 and 13 m/s. Velocity variations were obtained by changing the pump rotation speed. For each velocity, the acquisition device was located in all possible locations in the cavitation area, in order to record measurements with various void fractions.

Grid 2 creates much less cavitation than grid 1, so the values of $\bar{\alpha}$ are systematically lower than 5%. To investigate the influence of the flow velocity, only the data leading to void fractions in the range 1–3% were considered. It can be observed in Fig. 23 that nearly all values of the speed of sound are obtained in the range 10–20 m/s. Two measurements for which the celerity of sound exceeds 30 m/s (framed by an ellipse) correspond to void fraction close to 1%, while all others exceed 1.5%. This confirms that the mean flow velocity should not have any influence

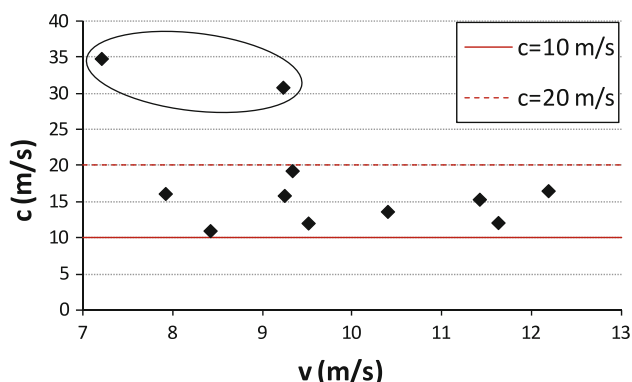


Fig. 23 Speed of sound according to mean flow velocity (grid 2)

on the values of the speed of sound obtained with the present acquisition device and post-processing.

6 Conclusion

An experimental technique that enables to produce a reasonably homogeneous two-phase flow area in a constant cross-section duct has been proposed and validated in this study. The flow homogeneity has been checked in various situations of air/water mixtures and cavitating flows, using an optical probe calibrated previously. The main objective of the work was the experimental determination of the wave celerity in a cavitating flow, according to the void fraction, in order to discuss the validity of some theoretical models available in the literature. For that purpose, a method based on three pressure transducers mounted flash along the pipe has been applied for the measurement of the speed of sound. Because very small values of celerity have been obtained when high void fractions are encountered, the effect of Mach number has been included in the post-treatment of the signals of the three transducers. This new methodology, which is based on an iterative process, has been developed and used for the purpose of the present work. The results demonstrate that the impact of the Mach number should be taken into account in configurations of high void fractions. The experimental results in cavitating flows are consistent with several theoretical models which do not include any effect of mass transfer, which suggests that the flow vaporization and condensation plays only a minor role in the compressibility of the liquid/vapor mixture. The present method may be improved in the future by using a more local device for the measurement of the speed of sound. A technique based on two hydrophones—one emitter and one receptor—located on opposite sides in a cross-section is currently developed. The objective is to use impulsions instead of periodical signals, in order to get rid of the spurious reflections that were observed when this technique was applied in the frame of the present study.

Acknowledgments The authors are very grateful to EDF and CETIM for their financial support of the present work, in the frame of French Industry Research Consortium for Turbomachinery (CIRT). They also express their gratitude to the technical staff of Arts et Metiers ParisTech, especially J. Choquet and P. Olivier, for their assistance.

References

- Abom M, Boden H (1988) Error analysis of two microphones measurements in ducts with flow. *J Am Acoust Soc* 2429–2438
- Arndt REA, Song CCS, Kjeldsen M, He J, Keller A (2000) Instability of partial cavitation: a numerical/experimental approach. In:

- Proceedings of 23rd symposium on naval hydrodynamics, Val de Reuil, France
- Bolpaire S (2000) Etude des écoulements instationnaires dans une pompe en régime de démarrage ou en régime établi. PhD Dissertation ENSAM, July 2000
- Brennen CE (2005) Fundamentals of multiphase flows. Cambridge University Press
- Costigan G, Whalley PB (1997) Measurements of the speed of sound in air-water flows. Chem Eng J 66:131–135
- Coutier-Delgosha O, Reboud JL, Delannoy Y (2003) Numerical simulation of unsteady cavitating flow. Int J Numer Methods Fluids 42(5):527–548
- Delannoy Y, Kueny J-L (1990) Two-phase flow approach in unsteady cavitation modelling. Cavitation and multiphase flow forum, ASME-FED vol 98, pp 153–158
- Gabillet C, Colin C, Fabre J (2002) Experimental study of bubble injection in a turbulent boundary layer. Int J Multiph Flow 28:553–578
- Gouse SW, Brown GA (1964) A survey of the velocity of sound in two-phase mixtures. ASME Paper 64-WA/FE-35
- Henry RE, Grolmes MA, Fauske HK (1971) Pressure pulse propagation in two-phase one- and two-component mixtures. Argonne National Laboratory, Rep. 7792
- Jakobsen JK (1964) On the mechanism of head breakdown in cavitating inducers. J Basic Eng Trans ASME 291–305
- Leroux J-B, Coutier-Delgosha O, Astolfi J-A (2005) A joint experimental and numerical analysis of mechanisms associated to unsteady partial cavitation. Phys Fluids 17(5), paper 052101
- Margolis DL, Brown FT (1976) Measurement of the propagation of long-wavelength disturbances through turbulent flow in tubes. J Fluids Eng 70–78
- Merkle CL, Feng J, Buelow PEO (1998) Computational modelling of the dynamics of sheet cavitation. In: Michel J-M, Kato H (eds) Proceedings of 3rd International Symposium on Cavitation, vol 2, pp 307–314
- Miles JH (1981) Acoustic transmission matrix of a variable area duct or nozzle carrying a compressible subsonic flow. J Acoust Soc Am 69(6):1577–1586
- Nguyen DL, Winter ERF, Greiner M (1981) Sonic velocity in two-phase systems. Int J Multiph Flow 7:311–320
- Stutz B, Reboud J-L (1997) Experiment on unsteady cavitation. Exp Fluids 22:191–198
- Stutz B, Reboud J-L (2000) Measurements within unsteady cavitation. Exp Fluids 29:545–552
- Testud P, Moussou P, Hirschberg A, Auréan Y (2007) Noise generated by cavitating single-hole and multi-hole orifices in a water pipe. J Fluids Struct 23:163–189
- Wallis GB (1969) One-dimensional two-phase flow. McGraw-Hill
- Wylie EB, Streeter VL (1978) Fluid transients. McGraw-Hill, New York